Downloaded from jnm.snmjournals.org by on March 15, 2017. For personal use only.

MRI-Based Correction for Partial-Volume Effect Improves Detectability of Intractable Epileptogenic Foci on ^{123}I-Iomazenil Brain SPECT Images

Hiroki Kato[1], Eku Shimosegawa[1], Naohiko Oku[2], Kazuo Kitagawa[3], Haruhiko Kishima[4], Youichi Saitoh[4], Amami Kato[5], Toshiki Yoshimine[4], and Jun Hatazawa[1]

[1]Department of Nuclear Medicine and Tracer Kinetics, Osaka University Graduate School of Medicine, Suita, Japan; [2]Department of Nuclear Medicine, Hyogo College of Medicine, Nishinomiya, Japan; [3]Department of Neurology, Osaka University Graduate School of Medicine, Suita, Japan; [4]Department of Neurosurgery, Osaka University Graduate School of Medicine, Suita, Japan; and [5]Department of Neurosurgery, Kinki University School of Medicine, Osaka-Sayama, Japan

^{123}I-Iomazenil brain SPECT has been used for the detection of epileptogenic foci, especially when surgical intervention is considered. Although epileptogenic foci exhibit a decrease in ^{123}I-iomazenil accumulation, normal cerebral cortices often exhibit similar findings because of thin cortical ribbons, gray matter atrophy, or pathologic brain structures. In the present study, we created ^{123}I-iomazenil SPECT images corrected for gray matter volume using MRI and tested whether the detectability of the epileptogenic foci improved. **Methods:** Seven patients (1 male patient and 6 female patients; mean age ± SD, 34 ± 17 y) with intractable epilepsy were surgically treated by resecting the cerebral cortex after surface electroencephalography. Histopathologic examination of the resected specimens and a good outcome after surgery indicated that the resected lesions were epileptogenic foci. These patients underwent ^{123}I-iomazenil SPECT and 3-dimensional T1-weighted MRI examinations before their operations. Each SPECT image was coregistered to the corresponding MR image, and its partial-volume effect (PVE) was corrected on a voxel-by-voxel basis with a smoothed gray matter distribution image. Four nuclear medicine physicians visually evaluated the ^{123}I-iomazenil SPECT images with and without the PVE correction. The SPECT count ratio of the suspected focus to the contralateral cerebral cortex was evaluated as an asymmetry index (%) based on the volume of interest. **Results:** The sensitivity, specificity, and accuracy of focus detection by visual assessment were higher after PVE correction (88%, 99%, and 98%, respectively) than before correction (50%, 92%, and 87%, respectively). The mean asymmetry index for the surgically resected lesions was significantly higher on the PVE-corrected SPECT images (22%) than on the PVE-uncorrected ones (16%) ($P = 0.006$). **Conclusion:** MRI-based PVE correction for ^{123}I-iomazenil brain SPECT improves the sensitivity and specificity of the detection of cortical epileptogenic foci in patients with intractable epilepsy.

Key Words: epilepsy; ^{123}I-iomazenil; SPECT; MRI; partial-volume effect

J Nucl Med 2008; 49:383–389
DOI: 10.2967/jnumed.107.046136

Iomazenil labeled with ^{123}I is a tracer that is specifically bound to central benzodiazepine receptors (*1*). Because epileptogenic foci exhibit a reduction in central benzodiazepine receptors (*2,3*), ^{123}I-iomazenil brain SPECT has been used to detect epileptic foci, especially when surgical intervention is considered (*3*). However, normal cerebral cortices often exhibit similar findings on ^{123}I-iomazenil SPECT because of thin cortical ribbons, gray matter atrophy, or pathologic brain structures. This limitation is caused by the partial-volume effect (PVE), which arises from the limited spatial resolution of the scanner. In small structures, the observed radioactivity concentration differs from the true concentration because of blurring of the counts out of the structure ("spill-out") and blurring of the counts into the structure from the surrounding radioactivity ("spill-in") (*4*).

In a previous study (*5*) examining patients with intractable mesial temporal lobe epilepsy arising from hippocampal sclerosis, the sensitivity of detecting pathologic hippocampi using ^{11}C-flumazenil PET was improved by PVE correction using MRI-based measurements of hippocampal volume. In the present study, we created ^{123}I-iomazenil SPECT images corrected for the whole-brain gray matter volume based on MRI measurements in patients with intractable partial epilepsy and tested whether the detectability of cortical epileptogenic foci improved.

MATERIALS AND METHODS

Patients

Seven patients with intractable epilepsy (1 male patient and 6 female patients; mean age ± SD, 34 ± 17 y) who met the following criteria were studied: no morphologic brain lesions other than small

Received Aug. 7, 2007; revision accepted Nov. 20, 2007.
For correspondence or reprints contact: Jun Hatazawa, MD, PhD, Osaka University Graduate School of Medicine, 2-2 Yamadaoka, Suita, 565-0871, Japan.
E-mail: hatazawa@tracer.med.osaka-u.ac.jp
COPYRIGHT © 2008 by the Society of Nuclear Medicine, Inc.

Downloaded from jnm.snmjournals.org by on March 15, 2017. For personal use only.

cystic lesions or suspected unilateral hippocampal atrophy (hippocampal sclerosis) visible on routine conventional MR images, surgical removal and histopathologic examination of suspected epileptogenic foci, improvement of patients' symptoms after surgery, and performance of ^{123}I-iomazenil brain SPECT and 3-dimensional (3D) T1-weighted MRI studies before operation.

The patients' clinical information is summarized in Table 1. All patients had complex partial seizures with or without generalization and were being treated with anticonvulsants. The Wada test, verbal magnetoencephalogram, or Edinburgh test was performed to determine the lateralization of verbal function or memory. All patients underwent surface electroencephalography or magnetoencephalography to identify the location and extent of the epileptogenic foci. All specimens resected during the operations were histopathologically investigated (Table 2). The histologic findings in 5 of 7 patients were nonspecific gliosis or neurodegeneration, and 1 patient (patient 3) was suspected of having astrocytoma. The outcome after surgery was evaluated on the basis of Engel's classification. The average follow-up period after surgery was 14 mo (range, 9–18 mo). Five patients were classified as Engel's classification I, and the remaining patients as Engel's classification III.

SPECT

In each subject, 167 MBq of ^{123}I-iomazenil were intravenously administered. Three hours after the injection, SPECT images were acquired while the subject rested supine on the scanning bed with eyes closed in a quiet room. SPECT was performed using a 4-head γ-camera (*6*) (Gamma View SPECT 2000H; Hitachi Medical Corp.) with a low-energy middle-resolution thin-section parallel-hole collimator. After the patient's head had been fixed on the headrest, the orbitomeatal line was detected using a laser-assisted device equipped with the γ-camera. The acquisition protocol was 20 s per step, with 64 collections over 360°, and the data were recorded in a 64 × 64 matrix. The raw SPECT data were transferred to a nuclear medicine computer (HARP 3; Hitachi Medical Corp.). The projection data were prefiltered using a Butterworth filter (cutoff frequency, 0.20 cycles per pixel; order, 10) and reconstructed into transaxial sections of 4.0-mm thickness in planes parallel to the orbitomeatal line. Attenuation correction was performed using Chang's method (*7*) with an optimized effective attenuation coefficient of 0.08 cm^{-1}.

PVE Correction

PVE was corrected using 3D T1-weighted MRI and a personal computer (Dell Dimension 8300; Dell Inc.) running Windows XP (Microsoft Corp.), as described in Figure 1. Thin-slice sagittal 3D T1-weighted MR images were produced using 3 types of MRI scanners: a Signa Excite 3.0 T, a Signa Excite HD 1.5 T (GE Yokogawa Medical Systems Ltd.), and a Magnetom Vision Plus 1.5 T (Siemens AG). In each case, a spoiled gradient echo sequence was used (echo time/repetition time: 1.928/8.632 ms, 1.820/8.552 ms, and 4.700/9.000 ms for the respective scanners; flip angle: 18, 18, and 12, respectively; acquisition matrix: all 256 × 256; slice thickness: all 1.4 mm). The acquired sagittal images were reformatted to axial images with a thickness of 1.4 mm.

The T1-weighted MR images were first segmented into gray matter, white matter, cerebrospinal fluid, or other compartments (skull and extracranial structures) using SPM5 (Wellcome Department of Imaging Neuroscience). This procedure yielded a Bayesian probability map for each tissue class based on a priori MRI information with an inhomogeneity correction for the magnetic field (*8*). Voxels were assigned into 3 tissue classes (gray matter, white matter, and cerebrospinal fluid) according to the maximum probability encountered for each voxel across the 3 datasets. These 3 tissue classes were subsequently put into binary form (given a value of 0 for absence of tissue or 1 for presence of tissue) (*9*).

The point-spreading function of the reconstructed SPECT images acquired with the low-energy middle-resolution thin-section parallel-hole collimator was assessed using a ^{123}I 1-mm-diameter line source in air, according to a previously described methodology (*6*). The binary maps for the gray matter were convoluted with a 3D gaussian function with a full width at half maximum of 12 × 12 × 12 mm, which was assumed to be the same as the point-spreading function of the reconstructed SPECT image, as described in previous studies (*10,11*). The resulting image was subsequently referred to as the smoothed gray matter map.

The ^{123}I-iomazenil SPECT images were coregistered to the smoothed gray matter maps using FMRIB's Linear Image Registration Tool (FLIRT) (*12*). In this procedure, the ^{123}I-iomazenil SPECT images were simultaneously reformatted to a matrix of the same size (256 × 256 × 256) as the referenced smoothed gray matter maps.

A binary volume image was created from the smoothed gray matter map as a mask image for the gray matter. The threshold for determining

TABLE 1
Characteristics of Subjects

Patient no.	Age (y)	Sex	Onset (y)	Duration (y)	Seizures/mo	Interval* (d)	Diagnosis	Anticonvulsants	MRI	Language dominancy
1	24	F	14	10	120	4	LTLE	CBZ, CLB	NP	L (Wada test)
2	65	F	43	22	30	2	MTLE	PHT	NP	Bilateral (Wada test)
3	44	F	40	4	30	2	LTLE	None	Small cyst in R ATL	Bilateral (Wada test)
4	14	F	3	11	5	10	MTLE	VPA, CBZ, PHT	NP	L (MEG study)
5	30	F	8	22	10	7	MTLE	CBZ, CLB, CZP	R HS	L (Wada test)
6	28	F	19	9	5	3	MTLE	VPA	L HS	L (Edinburgh test)
7	31	M	9	22	8	2	LTLE	CBZ, CLB, CZP	NP	R (Wada test)

*Between last seizure and SPECT study.

LTLE = lateral temporal lobe epilepsy; CBZ = carbamazepine; CLB = clobazam; NP = not performed; MTLE = mesial temporal lobe epilepsy; PHT = phenytoin; ATL = anterior temporal lobe; VPA = sodium valproate; MEG = magnetoencephalogram; CZP = clonazepam; HS = hippocampal sclerosis.

Downloaded from jnm.snmjournals.org by on March 15, 2017. For personal use only.

TABLE 2
Operations and Prognosis

Patient no.	Resected lesions	Histology	Prognosis*	Follow-up (mo)
1	L superior temporal gyrus, middle temporal gyrus (corticectomy/multiple subpial transection)	Gliosis	IIc	18
2	L hippocampus (multiple subpial transection), L superior temporal gyrus (corticectomy)	Gliosis	Ib	17
3	R anterior temporal lobe (tailored lobectomy), R hippocampus (hippocampectomy)	Astrocytoma	Ia–Ib	16
4	R hippocampus (hippocampectomy), temporal lobe (tailored corticectomy)	Gliosis, degeneration	Id	14
5	R hippocampus (hippocampectomy), anterior temporal lobe (tailored lobectomy), superior temporal gyrus (corticectomy)	Satellitosis	Ia	14
6	L hippocampus (hippocampectomy), amygdaloid (amygdaloidectomy)	Neurodegeneration	Ia	9
7	L posterior central gyrus, angular gyrus (selective corticectomy/multiple subpial transection)	Unknown	IIIa	9

*Engel's classification. Class I: free of disabling seizures (completely seizure-free since surgery [Ia], nondisabling simple partial seizures [Ib], some disabling seizures but free of disabling seizures for at least 2 y ["running down"] [Ic], generalized convulsion with antiepileptic drug withdrawal only [Id]). Class II: rare disabling seizures (rare disabling seizures since surgery [<3/y] [IIa], more than rare disabling seizures initially but only rare seizures for at least 2 y [IIb], nocturnal seizures only [IIc]). Class III: worthwhile improvement (significant reduction in seizure frequency [>75% reduction] [IIIa], prolonged seizure-free intervals amounting to greater than half the follow-up period of at least 2 y [IIIb]). Class IV: no worthwhile improvement (insignificant reduction, no change, or increase in seizure frequency).

the boundary of the binary volume image was set at 35% (an empirically determined value) of the maximum, which was the same as the threshold value used in a previous study (*10*). This mask image for the gray matter was then applied to the coregistered ^{123}I-iomazenil SPECT image. The masked ^{123}I-iomazenil SPECT image was then divided using the smoothed gray matter map on a pixel-by-pixel basis (Fig. 1).

Visual Assessment

Four experienced nuclear medicine physicians visually assessed the coronal images. The physicians were unaware of the patients' clinical information to avoid biases caused by differences in the amount of information available for each of the patients. The physicians visually evaluated the coronal ^{123}I-iomazenil SPECT images with and without PVE correction, presented in a random order, and noted the areas of epileptogenic foci, where the tracer uptake was reduced when compared with the corresponding contralateral regions. Decisions on the foci were made by joint agreement during a conference of the 4 physicians.

Patients without epileptogenic foci were excluded from the present study. Therefore, the sensitivity and specificity of focus

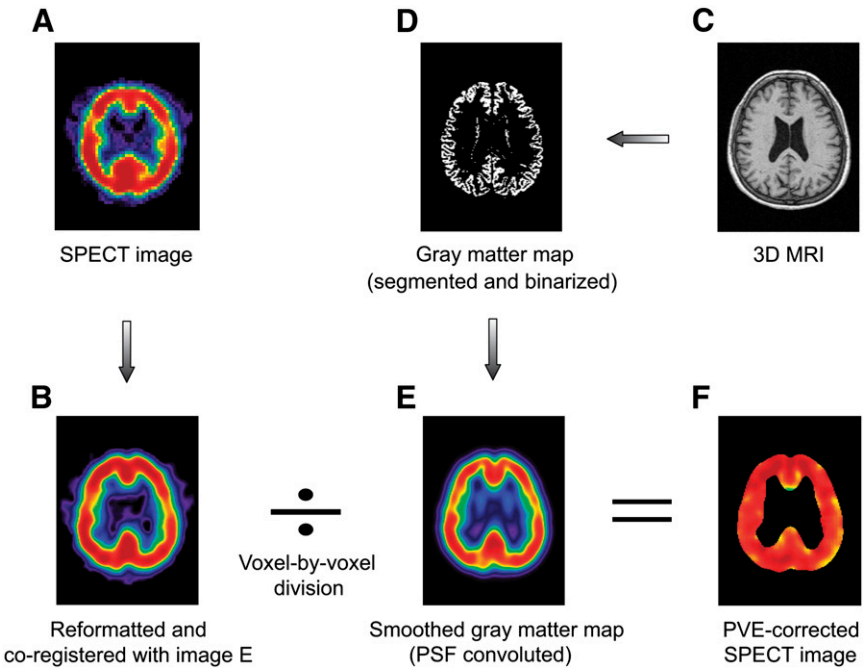


FIGURE 1. (A) ^{123}I-Iomazenil SPECT image. (B) Automatic coregistration of ^{123}I-iomazenil SPECT image with MR image via smoothed gray matter maps. Maps were simultaneously reformatted to matrix that was same size as referenced smoothed gray matter map. (C) 3D MR image obtained before operation. (D) MR image segmented into Bayesian probability map showing 3 tissue classes. Gray matter probability map was subsequently put into binary form (0 for absence of tissue, 1 for presence of tissue). (E) Binary map for gray matter convoluted with point-spreading function (PSF), which was assumed to be same as point-spreading function of SPECT scanner. (F) Smoothed gray matter map masked with threshold set to 35% of maximum voxel value. Coregistered ^{123}I-iomazenil SPECT image was divided using masked smoothed gray matter map on voxel-by-voxel basis.

Downloaded from jnm.snmjournals.org by on March 15, 2017. For personal use only.

detection were determined on a region-by-region basis. We divided the whole cerebrum into 18 bilateral blocks, as shown in Figure 2. We then assigned a binary value of positive or negative to each block, based on the visual assessment (i.e., positive for a focus, negative for no focus). We assumed that the resected lesions corresponded to the true epileptogenic foci and that unresected regions corresponded to the intact brain, because follow-up of surgical outcomes of the patients was good. Then, a true-positive result was defined as a positive result of visual assessment in a resected brain region, a true-negative result was defined as a negative result of visual assessment in an unresected brain region, a false-positive result was defined as a positive result of visual assessment in an unresected brain region, and a false-negative result was defined as a negative result of visual assessment in a resected brain region. The sensitivity, specificity, and accuracy of uncorrected or PVE-corrected SPECT images were calculated as follows:

$$\text{sensitivity} = \text{number of true-positive blocks}/\text{number of resected blocks},$$

$$\text{specificity} = \text{number of true-negative blocks}/\text{number of unresected blocks},$$

$$\text{accuracy} = (\text{number of true-positive blocks} + \text{number of true-negative blocks})/\text{number of total blocks}.$$

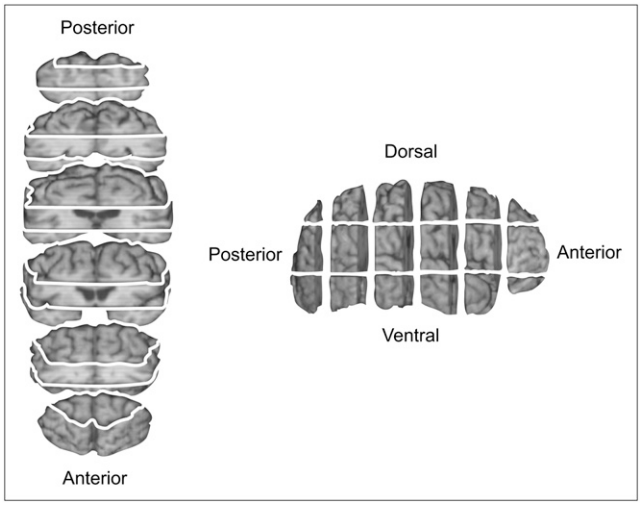


FIGURE 2. Whole cerebrum was divided into 18 bilateral blocks. A binary value of positive or negative was assigned to each block on the basis of visual assessment (i.e., positive for focus, negative for no focus). In this study, we assumed that resected lesions corresponded to true epileptogenic foci and unresected regions corresponded to intact brain because of good follow-up outcomes of patients after operations. Then, result of evaluation of each block was defined as follows. true-positive: positive result of visual assessment in resected brain region; true-negative: negative result of visual assessment in unresected brain region; false-positive: positive result of visual assessment in unresected brain region; false-negative: negative result of visual assessment in resected brain region.

Quantitative Assessment

First, the volume of interest (VOI) was established so as to include each resected lesion in reference to an MR image obtained after the operation (Fig. 3). If the VOI included a medial temporal lesion, it was divided into a medial temporal and a lateral part. Second, another VOI was made so as to contain each visually detected false-positive area on the uncorrected or PVE-corrected SPECT images that were coregistered with the MR images. For each of these VOIs, the corresponding contralateral VOI was also made in reference to the SPECT and MR images. The VOI counts of the uncorrected or the PVE-corrected SPECT images coregistered with the MR images were measured to evaluate quantitatively the sensitivity or specificity of the images of the epileptogenic foci. The asymmetry index (AI) for the ^{123}I-iomazenil SPECT count of the ipsilateral VOI A, C_A, and that of the contralateral VOI B, C_B, was calculated as follows:

$$\text{AI} = |C_A - C_B| \times 200/(C_A + C_B). \qquad \text{Eq. 1}$$

RESULTS

The sensitivity, specificity, and accuracy of focus detection by visual assessment were higher after PVE correction (88%, 99%, and 98%, respectively) than before correction (50%, 92%, and 87%, respectively). The AI values for the resected lesions are summarized in Table 3. The mean AI was significantly higher on the PVE-corrected SPECT images than on the uncorrected ones for the whole resected lesions (22%, 16%, $P = 0.006$), lateral parts of the resected lesions (20%, 12%, $P = 0.006$), and medial temporal parts of the resected lesions (25%, 20%, $P = 0.029$). In patients 2 and 7, true foci were not detected on the uncorrected SPECT images. In Table 4, the location, visual assessment, and AI for the false-positive regions are listed. The mean AI for the false-positive regions was significantly larger on the uncorrected images (12%) than on the PVE-corrected ones (4.8%) ($P < 0.001$).

The uncorrected and PVE-corrected SPECT images of typical patients are shown in Figure 4. A lateralized decrease in the counts was found on the PVE-corrected images in the areas corresponding to the resected lesions, although no laterality was seen on the uncorrected images (Fig. 4A). Conversely, a lateralized decrease in the counts was seen in the intact areas on the uncorrected images, whereas no laterality was found on the PVE-corrected images (Fig. 4B).

DISCUSSION

In the present study, we introduced a method for performing MRI-based PVE corrections on ^{123}I-iomazenil SPECT images. This method improved the accuracy with which epileptogenic foci can be detected in the cerebral cortices.

Inhibitory neural transmission is thought to be disturbed at epileptic foci (*13*). This hypothesis is supported by in vivo flumazenil PET (*14,15*) and iomazenil SPECT (*2,3*) studies. Previous studies have indicated a disproportion between the gray matter volume and the benzodiazepine receptor density in some epileptogenic foci (*3,16,17*). In patients with hippocampal sclerosis, changes in benzodiazepine receptor

Downloaded from jnm.snmjournals.org by on March 15, 2017. For personal use only.

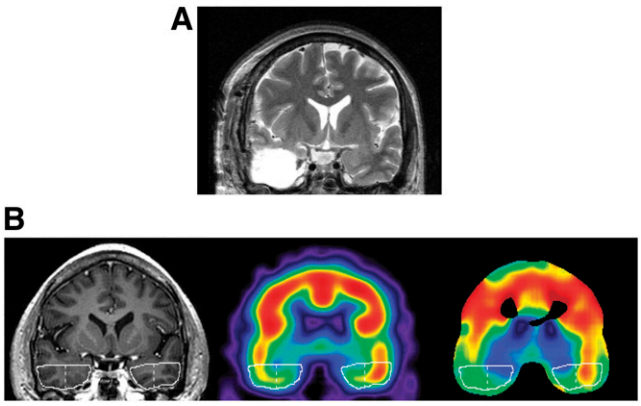


FIGURE 3. (A) MR image obtained after operation. (B) VOIs for resected brain lesions were established on 3D MR image (left) so as to include each resected lesion in reference to MR image obtained after operation. Corresponding contralateral VOIs were also established on same MR image. If VOI included medial temporal area, it was divided into lateral temporal part and medial temporal part (dashed line). Each VOI was applied to uncorrected (middle) and PVE-corrected (right) SPECT images coregistered to 3D MR image.

binding were detected in the hippocampus and the extrahippocampal neocortices, which appeared normal on MRI (*18*). Thus, identifying the location of epileptogenic foci and evaluating the extent of the area to be resected may be impossible using MRI alone. In the present study, a considerable number of true-positive lesions in the cerebral cortices appeared normal during the MRI study.

The nonspecific binding of iomazenil has been shown to account for a small proportion of all bound molecules (1%–3%) (*19*). According to an ex vivo study of nonhuman primates, iomazenil showed a predominantly high accumulation in the gray matter, with ratios of greater than 30:1 for gray matter to white matter (*20*). Thus, the distribution of iomazenil accumulation in the cerebrum is markedly influenced by the local volume of gray matter when a SPECT scanner with a limited spatial resolution is used. Nonpathologic laterality or an asymmetric distribution of gray matter volume on a certain slice may increase the risk of a false-positive result in side-by-side comparisons of iomazenil images.

The accurate determination of actual radiotracer concentrations in human gray matter in vivo is possible using MRI-based PVE corrections (*21,22*). In ethylcysteinate dimer SPECT, PVE correction made the regional cerebral blood flow distribution more homogeneous throughout the brain, with less intersubject variation than in the original distribution. Using this method for brain perfusion SPECT determines regional cerebral blood flow more accurately, even in healthy volunteers (*10*). As for ^{15}O-H_2O PET, PVE correction made it possible to estimate the regional cerebral blood flow accurately despite cortical atrophy both in Alzheimer's disease (*23*) and in normal aging (*24*). In ^{18}F-FCWAY (^{18}F-*trans*-4-fluoro-*N*-2-[4-(2-methoxyphenyl)piperazin-1-yl]ethyl-*N*-(2-pyridyl)cyclohexanecarboxamide) PET for the detection of foci in TLE patients, MRI-based PVE correction effectively eliminated artifacts related to PVE that were influenced by the local geometry of the gray matter and was useful for the extraction of pathologic serotonin 1A binding reduction (*25*).

The MRI-based PVE correction method used in the present study is similar to that used in previous studies (*5,10,23,26*). In this study, PVE was corrected for gray matter and other components (2-compartment method), although the PVE correction was performed for gray matter, white matter, and other brain structures (3-compartment method) in most of the previous studies. According to a previous validation study (*21*), the 2-compartment method is less sensitive to errors resulting from resolution mismatch between MRI and SPECT, misregistration, and missegmentation. Meanwhile, the 3-compartment method is capable of greater accuracy for absolute quantitative measures. The accumulation of ^{123}I-iomazenil in white matter is known to be markedly small; consequently, the spill-in of counts from the surrounding white matter to the gray matter voxels is negligible. For this application, the 2-compartment method is more suitable because the decrease in accuracy is small and the tolerance to errors in image processing is greater with the 2-compartment method than with the 3-compartment one.

TABLE 3
AI for VOI Counts in Resected Lesions

Patient no.	Resected lesions	Total resected lesions (AI [%])		Lateral part of lesions (AI [%])		Medial temporal part of lesions (AI [%])	
		Uncorrected	PVE-corrected	Uncorrected	PVE-corrected	Uncorrected	PVE-corrected
1	STG, MTG	2.2	10.8	2.2	10.8	—	—
2	ATL, MTL	7.4	13.6	5.6	13.0	−0.2	10.8
3	ATL, MTL	21.7	34.4	21.3	34.2	9.6	15.3
4	ITG, MTL	29.5	38.7	24.7	34.5	39.4	46.4
5	ATL, MTL	12.2	14.6	10.0	13.2	21.1	22.5
6	MTL	27.8	30.6	—	—	27.8	30.6
7	IPL	9.1	11.6	9.1	11.6	—	—

STG = superior temporal gyrus; MTG = middle temporal gyrus; ATL = anterior temporal lobe; MTL = mesial temporal lobe; ITG = inferior temporal gyrus; IPL = inferior parietal lobule.

Downloaded from jnm.snmjournals.org by on March 15, 2017. For personal use only.

TABLE 4
AI for VOI in False-Positive Areas

Patient no.	Location	Uncorrected		PVE-corrected	
		Visual assessment	AI (%)	Visual assessment	AI (%)
1	ATL	Positive	15.0	Positive	13.1
2	MTL-WM*	Positive	10.7	Negative	2.1
	SPL	Positive	10.3	Negative	4.1
3	OG	Positive	11.1	Negative	7.2
	IPL	Positive	14.6	Negative	1.4
	SPL	Positive	10.1	Negative	4.6
5	PHG	Positive	12.0	Negative	1.2
6	ATL	Positive	13.6	Negative	7.3
7	SPL	Positive	11.6	Negative	2.1
	MTL	Positive	11.9	Negative	4.7

*Contralateral to true focus.

ATL = anterior temporal lobe; MTL-WM = mesial temporal lobe white matter; SPL = superior parietal lobule; OG = orbital gyri; IPL = inferior parietal lobule; PHG = parahippocampal gyrus; MTL = mesial temporal lobe.

In this study, an increase in the AI of the resected lesions was shown after PVE correction in both the lateral part and medial temporal part of the resected lesions. This finding implies an increase in the volume of the gray matter or decrease in the volume of the adjacent white matter in the lesion areas, compared with that in the corresponding contralateral normal areas. In the previous study (*27*), an increase in the regional gray matter concentration in malformations of cortical development in patients with focal cortical dysplasia was detected by voxel-based morphometry. In addition, the local increase of the gray matter volume has been reported to coincide with that of the white matter volume, as detected by voxel-based morphometry, around pathologic sclerotic medial temporal lesions in cases of temporal lobe epilepsy (*28*). This phenomenon may, however, be controversial, and further detailed investigation is needed of the changes in the AI in pathologic medial temporal lesions associated with PVE correction.

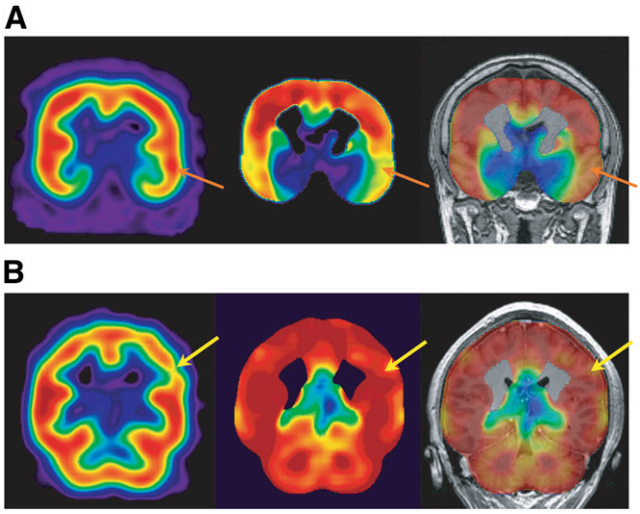


FIGURE 4. Typical SPECT images of 2 patients are shown. In each case, uncorrected SPECT image is on left, PVE-corrected SPECT image in middle, and PVE-corrected SPECT image coregistered to MR image on right. (A) Although no laterality could be found on uncorrected images, localized decrease in count on PVE-corrected images is distinct in areas corresponding to resected lesions. (B) No laterality was found on PVE-corrected images; unilateral decreased count, however, was found in intact areas on uncorrected images. Arrows indicate the true focus (red) or the false-positive region (yellow).

The present study had some limitations. First, the number of patients was too small to ensure statistical reliability. Second, some of the patients were taking anticonvulsants (e.g., clobazam) at the time of their ^{123}I-iomazenil SPECT examination, even though such drugs may influence iomazenil binding to a certain extent. Previous reports, however, have suggested that the extent of this influence is small (*3,29*). Thus, as far as intrasubject comparisons using the AI are concerned, the influence of anticonvulsants was thought to be negligible. Additionally, the temporary withdrawal of anticonvulsants solely for the purpose of SPECT can be harmful or impractical. From this viewpoint, our findings suggest that PVE corrections for ^{123}I-iomazenil SPECT remain effective even when the patient is taking anticonvulsants. Third, the brain structure images were obtained using 3 different types of MRI scanners. However, this protocol was not problematic in the present study because interscanner comparisons were not included in the analysis. Fourth, white matter activity was masked and eliminated during the process of PVE correction, although some cases of refractory focal epilepsy with heterotopia caused by neuronal migration disturbances have been reported to show a high flumazenil uptake in periventricular white matter (*30*). Because the evaluation of abnormal ^{123}I-iomazenil activity in white matter is quite difficult because of the higher activity spill-out from the adjacent gray matter, further study to solve this problem is needed. Fifth, the resolution of the present scanner was around 11 mm, although the current state-of-the-art SPECT scanner has a resolution of around 4–5 mm at full width at half maximum. We consider that the PVE correction in these scanners is effective to detect small cortical foci of epilepsy. Finally, we assumed that the unresected brain tissues were normal. Because this assumption cannot be proved, the accuracy of the true-negative and false-positive categorizations is limited.

CONCLUSION

PVE correction for ^{123}I-iomazenil brain SPECT images using the MRI-based gray matter volume improved the sensitivity and specificity at which cortical epileptogenic foci could be detected in patients with intractable epilepsy.

ACKNOWLEDGMENTS

We thank the staffs of the Department of Pathology, Osaka University Graduate School of Medicine, for their help with the histology; Dr. Yasuyuki Kimura, Dr. Katsufumi Kajimoto,

Downloaded from jnm.snmjournals.org by on March 15, 2017. For personal use only.

and Dr. Makiko Tanaka for their contribution to the SPECT data acquisition; and Yukio Nakamura and the staff of the Department of Nuclear Medicine and the cyclotron staff of Osaka University Hospital for their technical support in performing this study. This study was supported in part by a grant for molecular imaging project from the Japan Science Technology Agency.

REFERENCES

1. Beer HF, Blauenstein PA, Hasler PH, et al. In vitro and in vivo evaluation of iodine-123-Ro 16-0154: a new imaging agent for SPECT investigations of benzodiazepine receptors. *J Nucl Med.* 1990;31:1007–1014.
2. Morimoto K, Watanabe T, Ninomiya T, et al. Quantitative evaluation of central-type benzodiazepine receptors with [^{125}I]iomazenil in experimental epileptogenesis: II. The rat cortical dysplasia model. *Epilepsy Res.* 2004;61: 113–118.
3. Sata Y, Matsuda K, Mihara T, Aihara M, Yagi K, Yonekura Y. Quantitative analysis of benzodiazepine receptor in temporal lobe epilepsy: [^{125}I]iomazenil autoradiographic study of surgically resected specimens. *Epilepsia.* 2002;43: 1039–1048.
4. Hoffman EJ, Huang SC, Phelps ME. Quantitation in positron emission computed tomography: 1. Effect of object size. *J Comput Assist Tomogr.* 1979;3: 299–308.
5. Koepp MJ, Richardson MP, Labbe C, et al. ^{11}C-Flumazenil PET, volumetric MRI, and quantitative pathology in mesial temporal lobe epilepsy. *Neurology.* 1997;49:764–773.
6. Kimura K, Hashikawa K, Etani H, et al. A new apparatus for brain imaging: four-head rotating gamma camera single-photon emission computed tomograph. *J Nucl Med.* 1990;31:603–609.
7. Chang LT. A method for attenuation correction in radionuclide computed tomography. *IEEE Trans Nucl Sci.* 1978;25:638–643.
8. Ashburner J, Friston KJ. Voxel-based morphometry: the methods. *Neuroimage.* 2000;11:805–821.
9. Bencherif B, Stumpf MJ, Links JM, Frost JJ. Application of MRI-based partial-volume correction to the analysis of PET images of mu-opioid receptors using statistical parametric mapping. *J Nucl Med.* 2004;45:402–408.
10. Matsuda H, Ohnishi T, Asada T, et al. Correction for partial-volume effects on brain perfusion SPECT in healthy men. *J Nucl Med.* 2003;44:1243–1252.
11. Ibanez V, Pietrini P, Alexander GE, et al. Regional glucose metabolic abnormalities are not the result of atrophy in Alzheimer's disease. *Neurology.* 1998;50: 1585–1593.
12. Jenkinson M, Smith S. A global optimisation method for robust affine registration of brain images. *Med Image Anal.* 2001;5:143–156.
13. Savic I, Persson A, Roland P, Pauli S, Sedvall G, Widen L. In-vivo demonstration of reduced benzodiazepine receptor binding in human epileptic foci. *Lancet.* 1988;2:863–866.
14. Arnold S, Berthele A, Drzezga A, et al. Reduction of benzodiazepine receptor binding is related to the seizure onset zone in extratemporal focal cortical dysplasia. *Epilepsia.* 2000;41:818–824.
15. Juhasz C, Chugani DC, Muzik O, et al. Relationship of flumazenil and glucose PET abnormalities to neocortical epilepsy surgery outcome. *Neurology.* 2001;56:1650–1658.
16. Lamusuo S, Pitkanen A, Jutila L, et al. [^{11}C]Flumazenil binding in the medial temporal lobe in patients with temporal lobe epilepsy: correlation with hippocampal MR volumetry, T2 relaxometry, and neuropathology. *Neurology.* 2000; 54:2252–2260.
17. Hammers A, Koepp MJ, Richardson MP, et al. Central benzodiazepine receptors in malformations of cortical development: a quantitative study. *Brain.* 2001;124: 1555–1565.
18. Hammers A, Koepp MJ, Labbe C, et al. Neocortical abnormalities of [^{11}C]-flumazenil PET in mesial temporal lobe epilepsy. *Neurology.* 2001;56:897–906.
19. Videbaek C, Friberg L, Holm S, et al. Benzodiazepine receptor equilibrium constants for flumazenil and midazolam determined in humans with the single photon emission computer tomography tracer [^{123}I]iomazenil. *Eur J Pharmacol.* 1993;249:43–51.
20. Sybirska E, al-Tikriti M, Zoghbi SS, Baldwin RM, Johnson EW, Innis RB. SPECT imaging of the benzodiazepine receptor: autoradiographic comparison of receptor density and radioligand distribution. *Synapse.* 1992;12:119–128.
21. Meltzer CC, Kinahan PE, Greer PJ, et al. Comparative evaluation of MR-based partial-volume correction schemes for PET. *J Nucl Med.* 1999;40:2053–2065.
22. Muller-Gartner HW, Links JM, Prince JL, et al. Measurement of radiotracer concentration in brain gray matter using positron emission tomography: MRI-based correction for partial volume effects. *J Cereb Blood Flow Metab.* 1992;12: 571–583.
23. Meltzer CC, Leal JP, Mayberg HS, Wagner HN Jr, Frost JJ. Correction of PET data for partial volume effects in human cerebral cortex by MR imaging. *J Comput Assist Tomogr.* 1990;14:561–570.
24. Meltzer CC, Cantwell MN, Greer PJ, et al. Does cerebral blood flow decline in healthy aging? A PET study with partial-volume correction. *J Nucl Med.* 2000; 41:1842–1848.
25. Giovacchini G, Toczek MT, Bonwetsch R, et al. 5-HT 1A receptors are reduced in temporal lobe epilepsy after partial-volume correction. *J Nucl Med.* 2005;46: 1128–1135.
26. Koepp MJ, Woermann FG. Imaging structure and function in refractory focal epilepsy. *Lancet Neurol.* 2005;4:42–53.
27. Bonilha L, Montenegro MA, Rorden C, et al. Voxel-based morphometry reveals excess gray matter concentration in patients with focal cortical dysplasia. *Epilepsia.* 2006;47:908–915.
28. Bernasconi N, Duchesne S, Janke A, Lerch J, Collins DL, Bernasconi A. Whole-brain voxel-based statistical analysis of gray matter and white matter in temporal lobe epilepsy. *Neuroimage.* 2004;23:717–723.
29. Duncan S, Gillen GJ, Brodie MJ. Lack of effect of concomitant clobazam on interictal ^{123}I-iomazenil SPECT. *Epilepsy Res.* 1993;15:61–66.
30. Hammers A, Koepp MJ, Richardson MP, Hurlemann R, Brooks DJ, Duncan JS. Grey and white matter flumazenil binding in neocortical epilepsy with normal MRI: a PET study of 44 patients. *Brain.* 2003;126:1300–1318.

Downloaded from jnm.snmjournals.org by on March 15, 2017. For personal use only.

JNM The Journal of NUCLEAR MEDICINE

MRI-Based Correction for Partial-Volume Effect Improves Detectability of Intractable Epileptogenic Foci on ^{123}I-Iomazenil Brain SPECT Images

Hiroki Kato, Eku Shimosegawa, Naohiko Oku, Kazuo Kitagawa, Haruhiko Kishima, Youichi Saitoh, Amami Kato, Toshiki Yoshimine and Jun Hatazawa

J Nucl Med. 2008;49:383-389.
Published online: February 20, 2008.
Doi: 10.2967/jnumed.107.046136

This article and updated information are available at:
http://jnm.snmjournals.org/content/49/3/383

Information about reproducing figures, tables, or other portions of this article can be found online at:
http://jnm.snmjournals.org/site/misc/permission.xhtml

Information about subscriptions to JNM can be found at:
http://jnm.snmjournals.org/site/subscriptions/online.xhtml

The Journal of Nuclear Medicine is published monthly.
SNMMI | Society of Nuclear Medicine and Molecular Imaging
1850 Samuel Morse Drive, Reston, VA 20190.
(Print ISSN: 0161-5505, Online ISSN: 2159-662X)

© Copyright 2008 SNMMI; all rights reserved.

SNMMI SOCIETY OF NUCLEAR MEDICINE AND MOLECULAR IMAGING